Phase-sensitive imaging and phase tomography using X-ray interferometers

Atsushi Momose

Department of Advanced Materials Science, Graduate School of Frontier Sciences, The University of Tokyo
7-3-1 Hongo, Bunkyo-ku, Tokyo 113-0033, Japan
momose@exp.t.u-tokyo.ac.jp

Abstract: X-ray interferometry for imaging applications is discussed with a review of X-ray interferometric imaging activities reported to date. Phase measurement and phase tomography based on X-ray interferometry are also presented. Finally the advantage of X-ray interferometric imaging in comparison with other phase-sensitive X-ray imaging methods is discussed.

OCIS codes: (340.7450) X-ray interferometry; (340.7440) X-ray imaging

References and links

1. A. Momose and J. Fukuda, "Phase-contrast radiographs of nonstained rat cerebellar specimen," Med. Phys. **22**, 375-380 (1995).
2. A. Authier, *Dynamical theory of X-ray diffraction* (Oxford, New York, 2001).
3. U. Bonse and M. Hart, "An X-ray interferometer," Appl. Phys. Lett. **6**, 155-156 (1965).
4. A. Momose, "Demonstration of phase-contrast X-ray computed tomography using an x-ray interferometer," Nucl. Instrum. & Methods A **352**, 622-628 (1995).
5. A. Momose, T. Takeda, Y. Itai, K. Hirano, "Phase-contrast X-ray computed tomography for observing biological soft tissues," Nat. Med. **2**, 473-475 (1996).
6. T. Takeda, A. Momsoe, K. Hirano, S. Haraoka, T. Watanabe, Y. Itai, "Human carcinoma: early experience with phase-contrast X-ray CT with synchrotron radiation—comparative specimen study with optical microscopy," Radiology **214**, 298-301 (2000).
7. A. Momose, T. Takeda, Y. Itai, "Blood vessels: depiction at phase-contrast X-ray imaging without contrast agents in the mouse and rat—feasibility study," Radiology **217**, 593-596 (2000).
8. P. Becker and U. Bonse, "The skew-symmetric two-crystal X-ray interferometer," J. Appl. Crystallogr. **7**, 593-598 (1974).
9. A. Yoneyama, A. Momose, I. Koyama, E. Seya, T. Takeda, Y. Itai, K. Hirano, K. Hyodo, "Large-area phase-contrast X-ray imaging using a two-crystal X-ray interferometer," J. Synchrotron Rad. **9**, 277-281 (2002).
10. A. Momose and K. Hirano, "The possibility of phase-contrast X-ray microtomography," Jpn. J. Appl. Phys. **38**, Suppl. 38-1, 625-629 (1999).
11. A. Momose, I. Koyama, Y. Hamaishi, H. Yoshikawa, T. Takeda, J. Wu, Y. Itai, K. Takai, K. Uesugi, Y. Suzuki, "Phase-contrast microtomography using an X-ray interferometer having a 40-μm analyzer," J. Phys. IV **104**, 599-602 (2003).
12. U. Bonse and M. Hart, "An X-ray interferometer with Bragg case beam splitting and beam recombination," Z. Physik **194**, 1-17 (1966).
13. I. Koyama, H. Yoshikawa, A. Momose, "Phase-contrast X-ray imaging with a triple-Bragg-case interferometer," Jpn. J. Appl. Phys. **42**, 80-82 (2003).
14. Y. Kohmura, T. Ishikawa, H. Takano, Y. Suzuki, "Shearing X-ray interferometer with an X-ray prism," J. Appl. Phys. **93**, 2283-2285 (2003).
15. C. David, B. Nöhammer, H. H. Solak, E. Ziegler, "Differential X-ray phase contrast imaging using a shearing interferometer," Appl. Phys. Lett. **81**, 3287-3289 (2002).
16. A. Momose, S. Kawamoto, I. Koyama, Y. Hamaishi, K. Takai, Y. Suzuki, "Demonstration of X-Ray Talbot Interferometry," Jpn. J. Appl. Phys. **42**, L866-L868 (2003).
17. H. Talbot, "Facts relating to optical science," Phil. Mag. **9**, 401-407 (1836).
18. G. Schmahl, P. Guttmann, G. Schneider, B. Niemann, C. David, T. Wilhein, J. Thieme, D. Rudolph, "Phase contrast studies of hydrated specimens with the X-ray microscope at BESSY," in *X-Ray Microscopy IV*, V. V. Aristov and A. I. Erko, eds., (Chernogolovka, Russia, 1994) pp.196-206.
19. Y. Kagoshima, Y. Yokoyama, T. Niimi, T. Koyama, Y. Tsusaka, J. Matsui, K. Takai, "Hard X-ray phase-contrast microscope for observing transparent specimens," J. Phys. IV **104**, 49-52 (2003).

#2796 - $15.00 US Received July 29, 2003; Revised September 14, 2003

20. I. McNulty, J. Kirz, C. Jacobsen, E. H. Anderson, M. R. Howells, D. P. Kern, "High-resolution imaging by Fourier transform X-ray holography," Science **256**, 1009-1012 (1992).
21. W. Leitenberger and A. Snigirev, "Microscopic imaging with high energy X-rays by Fourier transform holography," J. Appl. Phys. **90**, 538-544 (2001).
22. N. Watanabe, H. Yokosuka, T. Ohigashi, H. Takano, A. Takeuchi, Y. Suzuki, A. Aoki, "Optical holography in the hard X-ray domain," J. Phys. IV **104**, 551-556 (2003).
23. B. Kaulich, T. Wilhein, E. Di Fabrizio, F. Romanato, M. Altissimo, S. Cabrini, B. Fayard, J. Susini, "Differential interferometric contrast X-ray microscopy with twin zone plates," J. Opt. Soc. Am. A **19**, 797-806 (2002).
24. P. P. Naulleau, K. A. Goldberg, S. H. Lee, C. Chang, D. Attwood, J. Bokor, "Extreme-ultraviolet phase-shifting point-diffraction interferometer: a wave-front metrology tool with subangstrom reference-wave accuracy," Appl. Opt. **38**, 7252-7263 (1999).
25. L. B. Da Silva, T. W. Barbee, Jr., R. Cauble, P. Celliers, D. Ciarlo, S. Libby, R. A. London, D. Matthews, S. Mrowka, J. C. Moreno, D. Ress, J. E. Trebes, A. S. Wan, F. Weber, "Electron density measurements of high density plasmas using soft X-ray laser interferometry," Phys. Rev. Lett. **74**, 3991-3994 (1995).
26. J. Filevich, K. Kanizay, M. C. Morconi, J. L. A. Chilla, J. J. Rocca, "Dense plasma diagnostics with an amplitude division soft X-ray laser interferometer based on diffraction gratings," Opt. Lett. **25**, 356-358 (2000).
27. F. Delmotte, M.-F. Ravet F. Bridou, F. Varnière, P. Zeitoun, S. Hubert, L. Vanbostal, G. Soullie, "X-ray-ultraviolet beam splitters for the Michelson interferometer," Appl. Opt. **41**, 5905-5912 (2002).
28. K. Tamasaku, M. Yabashi, T. Ishikawa, "X-ray interferometry with multicrystal components using intensity correlation," Phys. Rev. Lett. **88**, 044801 (2002).
29. D. Joyeux and F. Polack, "Carbon index measurement near K edge, by interferometry with optoelectronic detection," in *X-Ray Microscopy and Spectromicroscopy*, J. Thieme, G. Schmahl, D. Rudolph, E. Umbach, eds., (Springer, Berlin, 1998), pp. II.103-II.112.
30. D. Joyeux, R. Mercier, D. Phalippou, M. Mullot, S. Hubert, P. Zeitoun, A. Carillon, A. Klisnick, G. Jamelot, E. Béchir, G. de Lacheze-Murel, "An interferometric microimaging system for probing laser plasma with an X-ray laser," in *X-Ray Microscopy*, W. Meyer-Ilse, T. Warwick, D. Attwood, eds., AIP Conf. Proc. 507, 511-514 (2000).
31. W. Cash, A. Shipley, S. Osterman, M. Joy, "Laboratory detection of X-ray fringes with a grazing-incidence interferometer," Nature **407**, 160162 (2000).
32. T. Haga, H. Takenaka, M. Fukuda, "At-wavelength extreme ultraviolet lithography mask inspection using a Mirau interferometric microscope," J. Vac. Sci. Technol. B **18**, 2916-2920 (2000).
33. A. Momose, "Phase-contrast X-ray imaging based on interferometry," J. Synchrotron Rad. **9**, 136-142 (2002).
34. T. Takeda, A. Momose, J. Wu, Q. Yu, T. Zeniya, Thet-Thet-Lwin, A. Yoneyama, Y. Itai, "Vessel imaging by interferometric phase-contrast X-ray technique," Circulation **105**, 1708-1712 (2002).
35. S. Snigirev, I. Snigireva, V. Kohn, S. Kuznetsov, I. Schelokov, "On the possibilities of X-ray phase contrast microimaging by coherent high-energy synchrotron radiation," Rev. Sci. Instrum. **66**, 5486-5492 (1995).
36. S. W. Wilkins, T. E. Gureyev, D. Gao, A. Pogany, A. W. Stevenson, "Phase-contrast imaging using polychromatic hard X-rays," Nature **384**, 335-338 (1996).
37. P. Cloetens, W. Luding, J. Baruchel, D. Van Dyck, J. Van Landuyt, J. P. Guigay, M. Schlenker, "Holotomography: Quantitative phase tomography with micrometer resolution using hard synchrotron radiation x rays," Appl. Phys. Lett. **75**, 2912- (1999).
38. K. A. Nugent, D. Paganin, T. E. Gureyev, "A phase odyssey," in *Physics Today* (AIP, August 2001) pp. 27-32.
39. T. J. Davis, D. Gao, T. E. Gureyev, A. W. Stevenson, S. W. Wilkins, "Phase-contrast imaging of weakly absorbing materials using hard X-rays," Nature **373**, 595-598 (1995).
40. I. V. Ingal, E. A. Beliaevskaya, "X-ray plane-wave topography observation of the phase contrast from a non-crystalline object," J. Phys. D: Appl. Phys. **28**, 2314-2317 (1995).
41. D. Chapman, W. Thomlinson, R. E. Johnston, D. Washburn, E. Pisano, N. Gmür, Z. Zhong, R. Menk, F. Arfelli, D. Sayers, "Diffraction enhanced X-ray imaging," Phys. Med. Biol. **42**, 2015-2025 (1997).

1. Introduction

The wave nature of light gives rise to a variety of fascinating interferometric phenomena. For many years scientists have made considerable efforts to utilize this aspect so that today the field of optical interferometry is well established. The phase of the light revealed by an interferometer conveys information on the optical properties and/or geometrical features of materials, which cannot be accessed by simple intensity measurements. Interferometry is now indispensable in many areas of modern science and technology.

#2796 - $15.00 US Received July 29, 2003; Revised September 14, 2003

The success of optical interferometry has motivated us to develop interferometers for other types of waves such as X-rays, neutrons, electrons and even atoms. However, the construction of such interferometers is, in general, more complex than the construction of optical interferometers. All interferometers need a coherent beam with sufficient flux. The sources available for interferometry are therefore limited. In addition, the wavelengths of X-rays, neutrons, and electrons are shorter than light and therefore require much tighter alignment and greater mechanical stability of the components of the interferometers.

In the X-ray region, however, the development of synchrotron radiation sources has made it possible to use high-flux X-rays with sufficient coherency, and the technologies for fabricating and aligning various optical components for X-rays have progressed. As a result of this, a variety of X-ray interferometers have been operated successfully and used for X-ray interferometric imaging.

In the hard X-ray region, the interaction cross-section of the X-ray phase shift for low-Z elements is approximately three orders of magnitude larger than that of absorption [1]. This implies from a macroscopic point of view that the difference in the real part of the refractive index between two different materials consisting of low-Z elements is approximately three orders larger than the difference in the imaginary part of the refractive index. For instance, structures in biological soft tissues, which cannot be fully imaged with conventional X-ray imaging relying on absorption, can therefore be depicted without the need for staining by using X-ray interferometric imaging. For biological imaging, in which X-ray radiation damage is crucial, this capability of X-ray interferometric imaging has a distinct advantage.

The aim of this article is to review recent studies in phase-sensitive X-ray imaging and phase tomography using X-ray interferometers. The advantages of X-ray interferometric imaging are discussed in comparison with other phase-sensitive imaging methods: the propagation-based method and the diffraction enhanced imaging method.

2. Requirements for X-ray interferometry

In order to construct an X-ray interferometer, one needs to overcome the difficulties in ensuring: (1) the coherency of X-rays, (2) the coherent division of an X-ray beam, and (3) the stability of the optical path length.

2.1 Coherency

Synchrotron radiation is normally passed through a crystal monochromator for the selection of hard X-rays. X-rays within a specific energy band are extracted using Bragg diffraction. The energy resolution is in the region of 10^{-4} with a normal double crystal monochromator. With sophisticated crystal arrangements, the energy resolution can be easily increased to 10^{-5} implying a temporal coherence length of around 10 μm. In the case of soft X-rays, monochromatization is normally achieved with a grating monochromator whose energy resolution is typically 10^{-2}~10^{-3}. The influence of the lower energy resolution on the temporal coherency is compensated by the fact that the wavelengths are much longer than those of hard X-rays. In most cases, X-ray interferometric imaging is performed in a situation where the optical path difference is much smaller than 10 μm so that one need not pay particular attention to temporal coherency.

Spatial coherency is particularly important for X-ray interferometric imaging. When an X-ray source with poor spatial coherency is used, the coherency must be improved by placing a pinhole downstream of the source. For harder X-rays, however, a smaller pinhole is required, leading to fabrication difficulties.

Bragg diffraction at the hard X-ray monochromator also functions as a beam collimator. The angular aperture for the incident X-rays satisfying the Bragg diffraction condition is normally about 10 μrad. Therefore when the angular diameter of an X-ray source is larger than the angular aperture, the effective source size downstream of the monochromator is defined by this aperture. Thus a small part of the source can be selected without using a pinhole generating a beam with a spatial coherence length of about 10 μm.

#2796 - $15.00 US Received July 29, 2003; Revised September 14, 2003

There is some uncertainty regarding the available X-ray flux in such situations. Synchrotron radiation sources are brilliant enough even after the coherence filtering mentioned above. Moreover, synchrotron radiation available from recently constructed low-emittance electron storage rings is sufficiently spatially coherent as generated. The difficulty in ensuring the X-ray coherency required for interferometric imaging has thus been overcome.

2.2 Beam division

Next, one needs to divide a wave into at least two waves coherently. Wavefront division, amplitude division and polarization division are normally used in optical interferometry.

Wavefront division is simple, provided that a spatially coherent beam is available. Young's double slits, Fresnel's bimirrors, prisms, etc. are applicable for wavefront division even of X-rays. One disadvantage is that the field of view generated by using these devices is normally quite small.

Amplitude division is superior to wavefront division in that spatial coherency is not as essential as in the case of wavefront division. Crystals are used for amplitude division in the hard X-ray energy region. Using dynamical diffraction [2], an incident X-ray beam can be divided into a diffracted beam and a forward-diffracted beam. Conveniently enough, this process involves monochromatization and collimation to perform coherence filtering as mentioned above. In the soft X-ray region, crystals are not available. Instead, free-standing multilayers or gratings are used.

Polarization division has not been used in X-ray interferometry. In some spatial configurations of dynamical diffraction in a perfect crystal, polarization division is possible in principle [2]. Depending on the experimental requirements, polarization division would be an attractive option and should be studied in the future.

2.3 Stability

The most annoying difficulty in X-ray interferometry is the fluctuation of the optical path length. When the path difference between the interfering X-ray beams fluctuates by more than their wavelength, the corresponding shift of generated interference fringes exceeds the spacing of the fringes. If the time required to record the fringes is longer than the time constant of the fluctuation, fringe contrast is lost. In order to observe interference fringes, an interferometer must be stabilized to a level significantly within the X-ray wavelength during the measurement.

In the X-ray region this difficulty can be overcome using four different approaches: (1) the use of paraxial rays, (2) the use of monolithic crystal optics, (3) the development of a precise and stable stage for aligning optical components, and (4) instant image acquisition:

(1) The use of paraxial rays is effective because any instability in the system has a similar effect on all the optical path lengths in the interferometer and the effect of instability is therefore cancelled.

(2) The triple Laue-case (LLL) X-ray interferometer [3] shown in Fig. 1(a) consists of three parallel crystal lamellae with a constant spacing between them, functioning as beam splitter (S), mirror (M) and analyzer (A) under the Bragg diffraction condition and forming Mach-Zehnder type optical paths. The entire body of the interferometer is cut monolithically from a perfect silicon crystal ingot. The optical components are self-aligned and no tuning mechanism is needed.

(3) In crystal X-ray interferometers other than those using the monolithic approach, individual optical components are assembled as rigidly as possible and great attention is paid to the suppression of vibration. Although this task is laborious, even in the hard X-ray region a crystal interferometer has been developed, as described later.

(4) One can record interference fringes when an image is acquired with an exposure much shorter than the instability time constant. Soft X-ray laser sources and some undulator radiation sources of the third generation synchrotron radiation facilities meet this demand.

#2796 - $15.00 US Received July 29, 2003; Revised September 14, 2003

3. Interferometers developed for X-ray imaging

In this section, X-ray interferometers developed for imaging applications are described individually including those operating in the soft X-ray region.

3.1 LLL X-ray interferometer

The LLL X-ray interferometer shown in Fig. 1(a) is the most well-known for being of practical use, even functioning with a laboratory X-ray source. Because of its monolithic structure the Bragg diffraction condition is satisfied at the three lamellae simultaneously. The incident X-ray beam is divided into two beams at the beam splitter (S) by amplitude division, and these two beams are each divided into two beams by the mirror (M). The two converging beams are recombined by the analyzer (A). An interference pattern caused by a sample placed in one arm of the interferometer is observed downstream of the analyzer. As described later, the change in the wavefront is measured using the technique of phase-shifting interferometry, and furthermore three-dimensional imaging is attained in combination with X-ray computed tomography [4].

The contrast resolution of X-ray interferometric imaging using the LLL interferometer is attractive from a medical point of view because structures in soft tissue, such as cancerous lesions and blood vessels, can be revealed [5-7]. The size of the field of view of the monolithic LLL X-ray interferometer, however, is limited by the diameter of the crystal ingot from which the interferometer is fabricated. A floating-zone (FZ) silicon ingot is preferred to ensure its performance as an X-ray interferometer. However, as the maximum diameter of commercially available FZ silicon ingots is 15 cm, the maximum field of view attainable, taking the geometry into account, is 7 cm × 7 cm. Another disadvantage of the monolithic LLL X-ray interferometer especially for imaging a living body is that the interferometer is deformed by the heat radiated from the body, which is in close proximity to the crystal lamellae.

An X-ray interferometer consisting of two independent crystal blocks, as shown in Fig. 1(b), is a candidate for overcoming those disadvantages; in principle the field of view can be greater than 10 cm × 10 cm and an object can be placed at some distance from the lamellae. However, since the advantage of the monolithic configuration is relinquished, a precise stage is required to align the blocks. A skew-symmetric system shown in Fig. 1(b) is convenient because linear displacements between the blocks are independent of interference and substantially only one rotation axis is required for tuning [8]. However, sub-nanoradian stability must be achieved for the rotation.

The stage shown in Fig. 2(a) has been developed for the non-monolithic interferometer [9]. The precise rotation mentioned above was achieved by rotating the S2 table on the S1 table. The bottom of the S2 table was lined with lubricating sheets of polyterafluoroethylene and was constrained to glide on the S1 table around a fixed point. The influence of vibration was reduced by thus increasing the rigidity of the system. The rotation was driven with a laminated piezoelectric actuator, to which the applied voltage was controlled so that the interference fringes remained static. Without this control, the drift in the rotation axis resulted

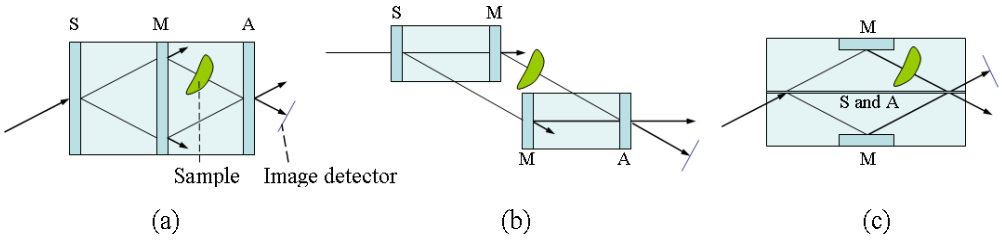

Fig. 1. Crystal X-ray interferometers used for interferometric imaging: (a) monolithic LLL X-ray interferometer, (b) interferometer consisting of two crystal blocks carrying two lamellae, and (c) BBB X-ray interferometer. S: beam splitter, M: mirror, A: analyzer.

#2796 - $15.00 US Received July 29, 2003; Revised September 14, 2003

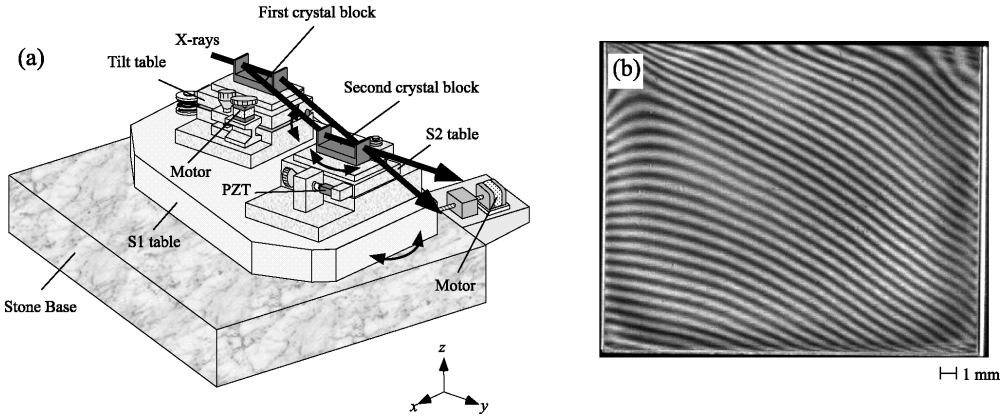

Fig. 2. X-ray interferometer consisting of two crystal blocks: (a) Stage for aligning the blocks and beam paths, (b) Interference pattern generated with this interferometer using 0.07-nm X-rays. From J. Synchrotron Rad. **9**, 277 (2002).

in interference fringes sweeping across the field of view. This feedback control was indispensable to make the interferometer stable for several hours.

As shown in Fig. 2(b), a 2.5 cm × 2.0 cm interference field was produced with the interferometer using 0.07-nm synchrotron X-rays from a vertical wiggler. With no object placed in the beam path, the fringes produced were due to imperfections in the interferometer. However, these fringes did not disturb imaging using the phase measurement technique described later.

In X-ray interferometric imaging with the crystal interferometers, the interference pattern is assumed to be a contour map of the phase shift caused by the sample. However, it should be noted that the spatial resolution is influenced by the analyzer located between the sample and the image detector [10]. According to the dynamical diffraction theory, the propagation vector of the X-ray inside the crystal is highly sensitive to its incident angle onto the crystal [2]. The ratio of the beam deflection angle inside the crystal to that outside is approximately 10^4:1. Since the phase shift at the sample causes refraction, which is normally neglected in conventional radiography, the resultant change in the angle of incidence to the analyzer is amplified in the analyzer causing image blurring. Recently, a LLL X-ray interferometer having an analyzer 40 μm in thickness [11], rather than the more conventional 1 mm, was fabricated in order to suppress the blurring effect. An image obtained with this interferometer will be presented later. Another approach using Bragg-case diffraction (BBB X-ray interferometer [12] shown in Fig. 1(c)) to suppress image blurring was also attempted [13]; *i.e.*, the beam passing through the sample does not go through the analyzer but is reflected by it reaching the image detector.

3.2 Differential hard X-ray interferometers

Differential X-ray interferometers, which generate fringes corresponding to contours of constant differential phase, have also been studied. The construction of these interferometers is comparatively easy because interfering beams are formed with paraxial rays.

A simple approach to differential X-ray interferometry has been taken using a prism [14] as shown in Fig. 3(a). Although the fact that the refractive index is almost unity in the hard X-ray region makes it difficult to use refractive optics, half of the wavefront of 0.1-nm X-rays was inclined by 23 μrad with an acrylic prism, without any embarrassing intensity loss, and interference could be observed 6.5 m downstream. Differential phase-contrast images of a sample placed 96 mm upstream of the image detection plane were successfully recorded.

Differential interferometers consisting of a pair of transmission gratings have also been studied. In the configuration of Fig. 3(b), two phase gratings designed to suppress the zeroth diffraction order and maximize the ±1st diffraction orders were aligned along the optical axis,

#2796 - $15.00 US Received July 29, 2003; Revised September 14, 2003

and a crystal was employed to select only the two beams that suffered +1st diffraction at G1 and -1st diffraction at G2 sequentially and -1st at G1 and +1st at G2 [15]. The interference between the two beams generates differential phase contrast of a sample placed in front of G1.

Another similar approach shown in Fig. 3(c) is X-ray Talbot interferometry [16], based on the Talbot effect [17] caused by a grating under spatially coherent illumination. It is a characteristic of the Talbot effect that one can observe the appearance and disappearance of the image corresponding to the pattern of the grating along the optical axis. Talbot interferometry employs two gratings normally with the same period. As shown in Fig. 3(c), one grating (G2) is placed at a position where the pattern of the other grating (G1) is reproduced by the Talbot effect. Moiré fringes are generated by superposition if the two gratings are slightly inclined. The differential phase caused by a sample placed in front of G1 is detected by moiré-fringe bending.

It should be noted that the interferometers shown in Figs. 3(b) and 3(c) employ wavefront division but the field of view is not limited. In addition, since paraxial X-rays are used, the alignment of the optics is easy. Provided that large gratings are fabricated, medical image diagnoses would be suitable applications for these interferometers.

3.3 Combination with focusing optics

For high-resolution interferometric imaging, combination with focusing optics is

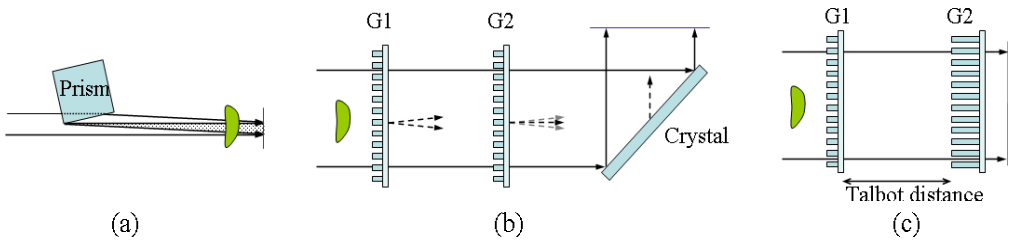

Fig. 3. Differential X-ray interferometers using a prism (a) and gratings (G1, G2) (b), (c).

straightforward. In addition, image formation should be considered with reference to the wave optics, while images obtained from the interferometry described above are normally interpreted by geometrical optics. Thus, this area of interferometric imaging relates more to holography or phase-contrast microscopy.

In the X-ray region, the Fresnel zone plate is the most developed focusing device used in microscopic imaging. In fact, Zernike's X-ray microscopes [18,19] and X-ray Fourier transform holography [20-22] are studied with zone plates. Here, a recent activity using a twin zone plate [23], shown in Fig. 4(a), is described. Zone plate patterns were formed on both sides of a substrate, but slightly displaced from each other. When the twin zone plate is illuminated coherently, two focal spots and therefore two spherical waves are formed and an interference field is generated. When the twin zone plate is used as an objective lens, differential phase contrast is generated at the image plane.

The quality of the focusing optics affects the performance of high-resolution X-ray imaging. X-ray interferometry can also be used for evaluating focusing optics with the setup [24] shown in Fig. 4(b). A transmission grating as a beam splitter is placed in front of the test optic, and two diffraction orders are extracted through a mask at the image plane of the test optic. The interference caused by the beams passing through the mask is detected showing imperfections in the test optic.

#2796 - $15.00 US Received July 29, 2003; Revised September 14, 2003

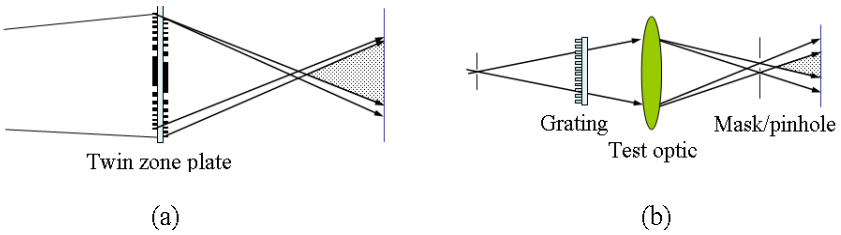

Fig. 4. X-ray interferometry with focusing optics. Using a twin zone plate (a), two focal spots have been formed generating an interference field downstream. When the twin zone plate is used as an objective lens, a differential phase-contrast image is obtained. Using a transmission grating, an interferometer (b) for testing focusing optics has also been developed.

3.4 Interferometers with instant image acquisition

As mentioned previously, one approach for overcoming the stability of an interferometer is instant image acquisition. This has been attained in soft X-ray interferometry using a soft X-ray laser because of its short pulse width and high peak brilliance. Figure 5 shows interferometers operated successfully mainly for plasma diagnosis, using free-standing multilayers [25] or gratings [26] for splitting and recombining beams. Recently a Michelson interferometer has also been operated using a free-standing multilayer [27]. Although all the optical elements, including the mirrors, were probably vibrating, the exposure time was much shorter than the period of vibration allowing the acquisition of a stop-motion picture of the fringes.

Instant image acquisition has also been performed with undulator hard X-rays [28]. Interference fringes were observed using an interferometer consisting of two independent crystal blocks, as shown in Fig. 1(b), with a 2-ms exposure. This achievement suggests that a variety of X-ray interferometers would be operated without requiring high stability using undulator sources at third-generation synchrotron radiation facilities and especially using X-ray free-electron laser sources in the near future.

It should be noted, however, that the correlation between instantly obtained images with a certain time interval is occasionally lost. Stability is therefore still important for applications, such as phase-shifting interferometry, that require multiple images recorded sequentially.

3.5 Other soft X-ray interferometers

For soft X-ray interferometry using synchrotron radiation, the interferometers shown in Fig. 6 are studied. The use of grazing-incidence mirrors would be a simple approach in this energy region. Interferometers using a Fresnel's bimirror have been operated successfully [29,30]. In X-ray astronomy, an X-ray interferometer employing multiple flat mirrors has also been studied to achieve ultra-high resolution [31]. A free-standing multilayer was also used to assemble a stable interferometer. Figure 6(b) shows a Mirau interferometer operated in combination with Schwarzschild optics [32]. Despite the fact that paraxial rays were not used in this configuration, its successful operation is a notable achievement.

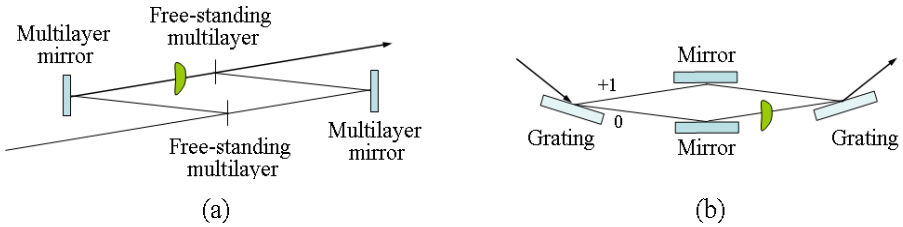

Fig. 5. X-ray interferometers using free-standing multilayers (a) or gratings (b) for amplitude division. Interference fringes could be observed by using a single shot of soft X-ray laser.

#2796 - $15.00 US Received July 29, 2003; Revised September 14, 2003

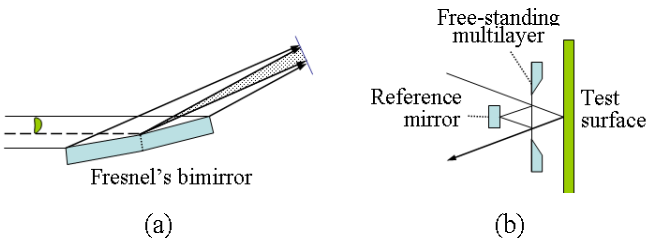

Fig. 6. Soft X-ray interferometers using synchrotron radiation. By using Fresnel's bimirror (a), a comparatively stable interferometer has been developed. Operation of a Mirau interferometer (b) with a free-standing multilayer is a notable achievement.

4. Phase tomography

4.1 Phase measurement

A simple example of the use of X-ray interferometers is in the recording of interference images on X-ray films. In practice, however, X-ray interferometers possess imperfections and generate a built-in fringe pattern, leading to confusion in the analysis of the structure of a sample. Even in a perfect interferometer, when the phase shift caused by the sample significantly exceeds 2π, it is difficult to grasp the shape of the wavefront from an interference pattern. Furthermore, amplitude contrast also occasionally coexists in interferometric images.

Phase measurement is therefore a meaningful next step for quantitative understanding of the wavefront. Several X-ray interferometers described in the previous section actually have the capability of phase measurement. The LLL X-ray interferometer was initially used for this purpose.

The fringe scanning method (in other words, the phase-shifting interferometry) and the Fourier transform method are applicable to the LLL X-ray interferometer system [1,7,33]. In

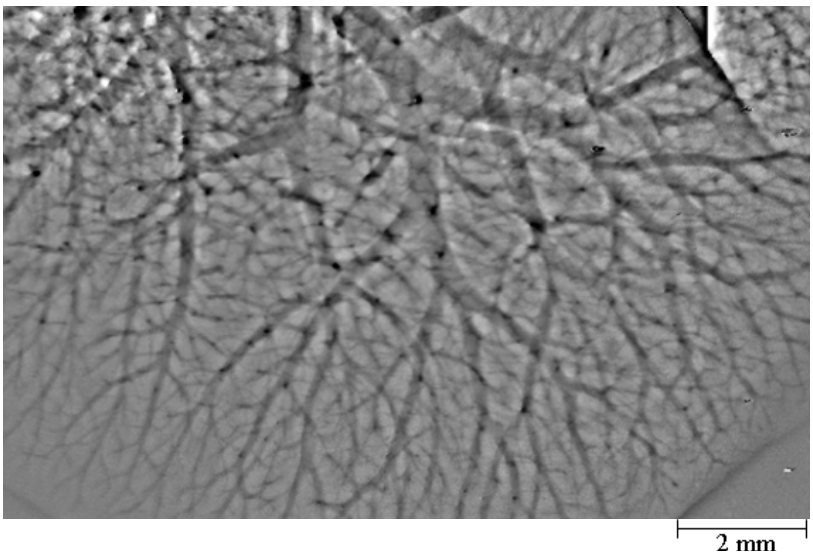

Fig. 7. Phase map measured with 0.07-nm X-rays by means of the fringe scanning method using the LLL X-ray interferometer. Blood vessels in a mouse liver were depicted by replacing blood with physiological salt solution. The contrast caused by the thickness variation of the liver has been removed by image processing.

#2796 - $15.00 US Received July 29, 2003; Revised September 14, 2003

the fringe scanning method, a tunable phase shifter is used and a spatial distribution of the phase shift, or a phase map, is obtained from several interference images recorded by a stepwise change of the phase difference between the two arms. In the Fourier transform method, carrier fringes are introduced with a wedge phase shifter. A phase map is obtained by Fourier filtering. The amplitude contrast, which is also present in the interferometric image, is removed by using these methods. The influence of the built-in fringes is pre-recorded as a background phase in the absence of a sample. The true phase shift caused by the sample is obtained by subtracting the background phase from the measured phase image.

The measurement of differential phase has also been performed with the Talbot interferometer (Fig. 3(c)) [16]. The G2 was moved in the direction parallel to the spatial modulation in order to perform the fringe scanning method. Similarly, differential phase measurement has been performed with the setup shown in Fig. 3(a) by moving the prism in the direction perpendicular to the optical axis [14].

When amplitude-contrast imaging is performed with N photons per pixel, the contrast resolution is proportional to $N^{-1/2}$ if other factors are ideal. It should be noted that the contrast resolution in the phase measurements is also proportional to $N^{-1/2}$. This implies that the difference between the cross-sections of absorption and phase shift, which is about a thousand times for low-Z elements in the hard X-ray region, is reflected directly in the contrast resolution. This has made it possible to observe structures in biological soft tissues using the LLL X-ray interferometer without using contrast media. In addition, when contrast media are used for selective imaging in a phase-sensitive mode, one can select a variety of materials for this purpose. For instance, vascular imaging of a mouse liver has been demonstrated by replacing blood with physiological salt solution [34], as shown in Fig. 7.

4.2 Tomographic reconstruction

X-ray phase measurements permit three-dimensional imaging using a tomographic technique. Assuming that the phase map corresponds to a projection of the refractive index of a sample, a three-dimensional distribution of the refractive index in the sample is revealed by processing the phase maps obtained in multiple projection directions. Such X-ray phase tomography has been achieved with an LLL X-ray interferometer [4]. As mentioned, the two crystal interferometer described in Fig. 2(a) was fully stable and was also dedicated to the measurement of phase tomography for a sample 10 mm in diameter [13].

Figure 8 is a tomographic image of the tissue of a rat kidney obtained with 0.1-nm X-rays using a LLL X-ray interferometer with a 40-μm analyzer [6]. The sample was observed in formalin and the image mapped the difference in the refractive index between the tissue and formalin. Tubules in the tissue, a part of which was clogged by protein, were resolved without using contrast media. Glomeruli were also clearly revealed.

The standard deviation of the noise in the phase tomogram shown in Fig. 8 was 1.8×10^{-9}. The refractive index decrement from unity is approximately proportional to the mass density, and the value for water is 1.5×10^{-6}. Therefore, the sensitivity of this phase tomography to density deviation is estimated from these values to be 1.2 mg/cm^3.

5. Advantages of X-ray interferometric imaging

Besides X-ray interferometry, the propagation-based method [35-38] and the diffraction enhanced imaging method [39-41] have also been studied for phase-sensitive X-ray imaging. The propagation-based method generates contrast caused by Fresnel or Fraunhofer diffraction by placing a sample and an image detector with a moderate separation. This method is of great advantage to high-resolution imaging because no optical components are needed, provided that a coherent X-ray source is available. The diffraction enhanced imaging method employs an analyzer crystal downstream of a sample to select the refracted X-rays from the sample. By means of dynamical X-ray diffraction at the analyzer, a μrad angular resolution is achieved in filtering X-rays deflected by refraction.

#2796 - $15.00 US Received July 29, 2003; Revised September 14, 2003

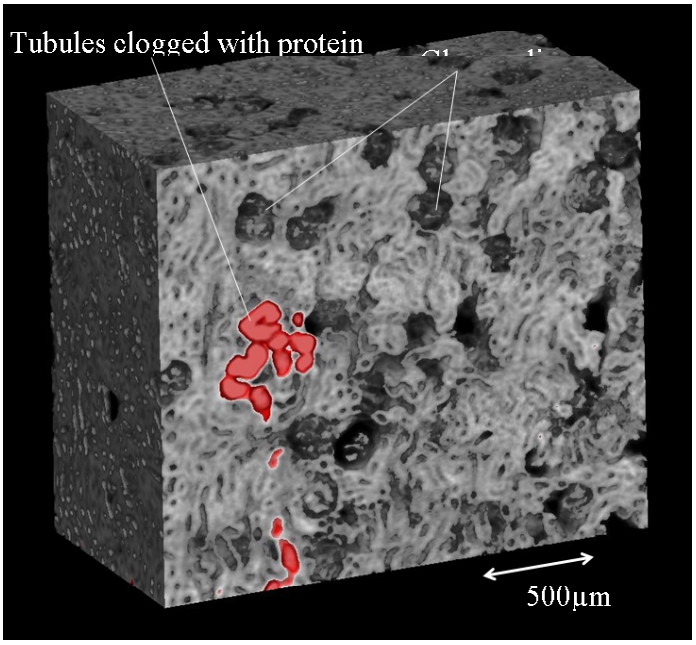

Fig. 8. The tissue of a rat kidney measured by phase tomography with 0.1-nm X-rays using the LLL X-ray interferometer with a 40-μm analyzer.

According to the principles of contrast generation by the propagation-based and diffraction enhanced imaging methods, stronger contrast is generated at structural boundaries where the variations of refractive index are larger inducing steeper phase gradients. In sensing shallower phase gradients, however, these methods are not effective. On the other hand, the interferometric methods, particularly those using the Mach-Zehnder type configuration, are suitable in this situation, because the interference fringe spacing becomes larger for shallower phase gradients. For instance, when 0.1-nm X-rays are deflected by 1 μrad, interference fringes with 0.1-mm spacing are generated, which are easily resolved with a normal X-ray image detector. The less the deflection is, the larger the fringe spacing.

The beam deflection caused by the structures in biological soft tissue is normally much lower than 1 μrad, and therefore observation of such structures by either the propagation-based or diffraction enhanced imaging methods is not easy. X-ray interferometric imaging is thus a unique approach for revealing soft structures. The density resolution of the phase tomography discussed in the previous section is attributable to this fact.

6. Summery

Owing to the difficulties in ensuring the coherency of X-rays, the coherent division of an X-ray beam and the stability of the optical path length, the construction of an X-ray interferometer is not as practicable as the construction of visible light interferometers. Nevertheless, various attempts at X-ray interferometric imaging, including phase tomography, have been reported, since the remarkable high-sensitivity that can be achieved with X-ray interferometry has the attraction of enabling unique observations to be made. As mentioned, among phase-sensitive X-ray imaging methods, the sensitivity of X-ray interferometric imaging should be emphasized. There is no doubt that the development of optical elements and coherent X-ray sources, including X-ray free electron lasers, will accelerate further the research into X-ray interferometric imaging and will also promote the discovery of new interferometric techniques other than those introduced in this article. The application of X-ray interferometric imaging, in fields ranging from microscopy to radiography, thus has great potential.

#2796 - $15.00 US Received July 29, 2003; Revised September 14, 2003

Acknowledgments

The images shown in Figs. 7 and 8 were obtained by the author in collaboration with Drs. T. Takeda, J. Wu, Y. Itai, A. Yoneyama, I. Koyama, Y. Suzuki with the technical assistance of Mr. Y. Hamaishi and Mr. K. Takai, under support from the Special Coordination Funds from the Ministry of Education, Calculation, Sports, Science, and Technology of Japan. The measurements using synchrotron radiation were performed under proposal number 99S2-002 approved by the High Energy Accelerator Research Organization, Japan, and the approval (2003A0459-NML2-np) of the committee of SPring-8, Japan.

#2796 - $15.00 US Received July 29, 2003; Revised September 14, 2003